

Experimental, DFT and QSAR models for the discovery of new pyrazines corrosion inhibitors for steel in oilfield acidizing environment

I. B. Obot* and S. A. Umoren

Center of Research Excellence in Corrosion, Research Institute, King Fahd University of Petroleum and Minerals, Dhahran 31261, Saudi Arabia

*E-mail: obot@kfupm.edu.sa

Received: 18 December 2019 / Accepted: 18 March 2020 / Published: 10 August 2020

Eight (8) pyrazine derivatives were tested as mild steel corrosion inhibitors in a simulated oil field acidizing environment. Immersion tests and DFT calculations were adopted for the study. Immersion tests were carried out at 0.2 wt. % inhibitor concentration at 25°C for a total duration of 24 h. The results showed that all the pyrazine derivatives tested protected the steel to various extents in the acid medium. Pyrazine carboxamide (Pyrazine E) exhibited the highest inhibition efficiency among the pyrazine derivatives investigated. The resulting molecular descriptors obtained from DFT calculations were correlated with the experimental inhibition efficiency to develop QSAR model. Multiple linear regression was utilized to correlate the inhibition efficiency with the molecular descriptors at a 95% confidence interval. This work revealed that the inhibition efficiencies of the studied pyrazine molecules were influenced by their E_{LUMO} , dipole moment (DM) and the molecular volume (MV). Based on the QSAR model developed, four new pyrazine derivatives were designed, and their inhibition efficiencies predicted.

Keywords: DFT; QSAR; pyrazine derivatives; corrosion inhibition efficiency; Step wise regression.

1. INTRODUCTION

The selection of corrosion inhibitors is mostly done through trial and error in synthesis and experimentation. It is vital to be able to investigate mechanisms of corrosion inhibition and the effect of the various groups attached using theoretical inhibition approach. This will provide a theoretical guidance for designing corrosion inhibitors. Organic compounds containing heteroatoms such as N, S, or O are effective corrosion inhibitors for many metals and alloys [1]. Addition of these organic molecules to the corrosive media helps in impeding corrosion [2]. The molecules normally form complexes by adsorbing to the metal surface [3–5].

Corrosion inhibitors protect the metal surface through molecular interaction leading to physical or chemical adsorption [6]. Heterogenous atoms with triple bonds and aromatic rings can form good coordination bonds with metal surfaces. The higher the strength of the coordination bond, the higher the inhibition efficiency. The drive toward the use of eco-friendly corrosion inhibitors led to numerous studies focused on heterocyclic compounds and those containing nitrogen are considered to be effective inhibitors [7–11]. Heterocyclic compounds containing nitrogen atoms in their structure such as quinoline, indole, pyridine, benzimidazole, pyridine and their various derivatives have been proven as efficient steel corrosion inhibitors [12–15].

Pyrazine is an important group of heterocyclic compounds [16,17] due to its diverse uses. Pyrazine and its derivatives finds wide applications in organic photovoltaics and organic light emitting diodes [18,19], flavoring in food [20,21], fragrances [22], pharmaceutical [23,24], agro-based chemicals, ligands [25] and anti-diabetic drugs [26]. Information regarding antifungal, antituberculosic and cytotoxicity of pyrazines have been widely reported [27–31]. Various pyrazine derivatives have been shown to be effective corrosion inhibitors in acid environment by several authors [32,33]. Notwithstanding these studies, specific mechanisms have not been supported experimentally. This difficulty in obtaining experimental evidence is often as a result of the complexity of the real environmental conditions surrounding the inhibitor, complications in extracting information regarding inhibitor and metal interface on atomic level experimentally and also due to the very low concentrations of these inhibitors utilized in experimental studies (in ppm levels) [34].

To address these issues, quantum chemical calculations can be very useful in explaining the corrosion inhibition mechanisms at the atomic level. Quantum chemical calculation was shown to be a powerful tool in corrosion inhibition studies and has been widely utilized in studying reaction mechanisms [35–41]. The relationship that characterizes the structure properties of molecules and their activities on a quantitative basis is structure–activity relationship (QSAR). QSAR does not only correlate and predict the physical and chemical properties of the molecules but also plays a significant role in their effective evaluation. The use of QSAR in corrosion inhibition study has been reported by several authors [42–47]. Molecular descriptors have an advantage since they are not closely restricted to related molecules, they are obtained without recourse to experimentation.

The aim of this work is to study the correlation between corrosion inhibition efficiency and molecular descriptors of 8 pyrazine derivatives. Weight loss measurements were used to evaluate the experimental corrosion efficiencies of the molecules. Quantum chemical study of 8 pyrazine molecules was performed at B3LYP/6-31G** level theory to evaluate the various molecular parameters of the molecules. The molecular parameters obtained were used to develop QSAR model for predicting the corrosion inhibition efficiency of molecules based on the pyrazine backbone. This information was further used to design corrosion inhibitors based on pyrazine moiety and their corrosion inhibition efficiency predicted based on the QSAR model developed.

2. EXPERIMENTAL DETAILS

2.1. Materials, Reagent and Inhibitors

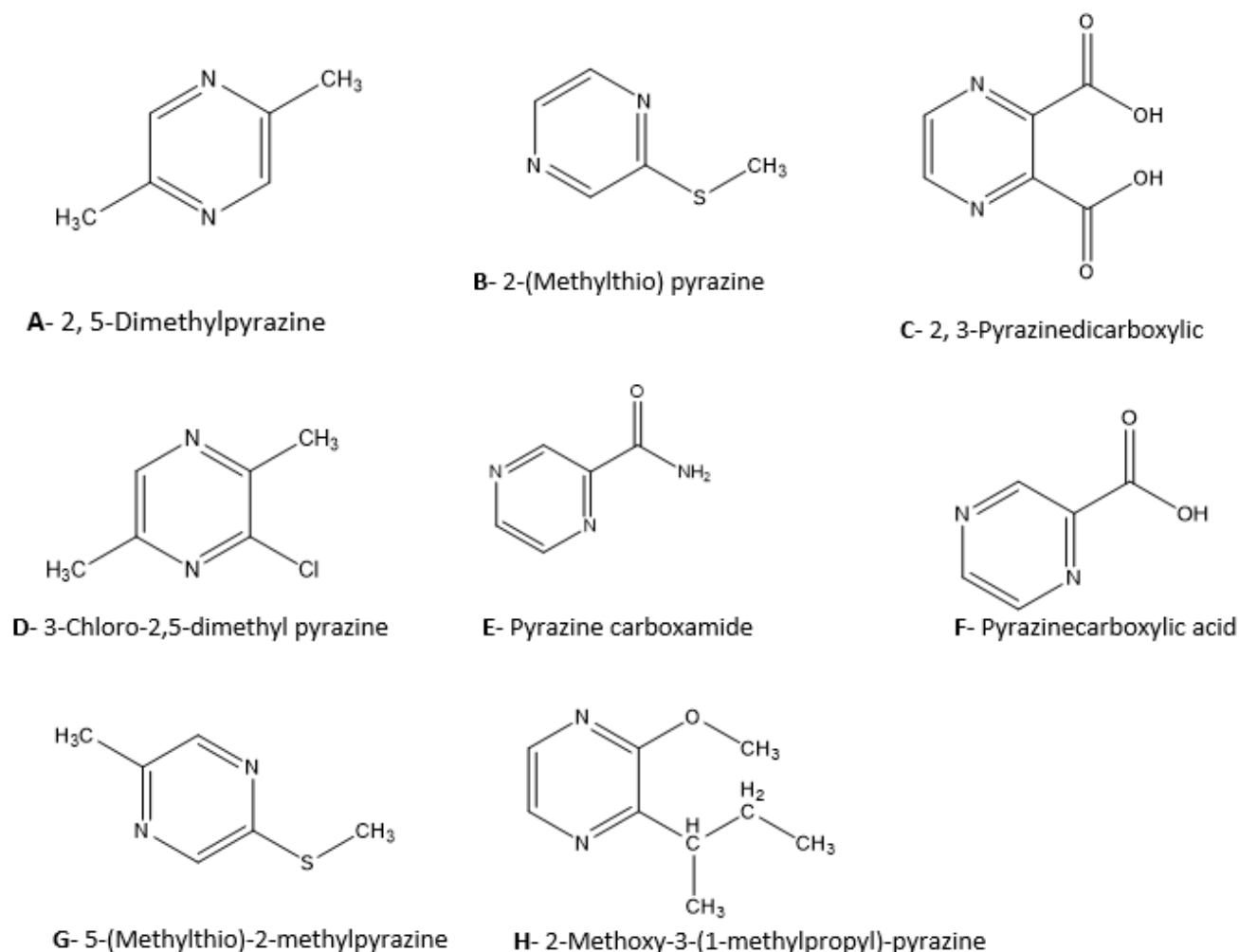


Figure 1. Names, abbreviations and 2 D-molecular structures of the investigated eight (8) pyrazine molecules.

The weight loss coupons were cut from a typical API X60 steel pipeline for this work. The coupons were cut into the dimension of 3×3 cm. Grinding and polishing were accomplished by utilizing emery papers with grit sizes ranging from 120, 240, 320, 400, 600 to 800. After grinding and polishing, the coupons were cleaned ultrasonically using acetone. The coupons were finally dried in air prior to immersion. Analytical grade HCl (purity-37 %) obtained from Sigma Aldrich was diluted to 15 % HCl acid with distilled water. All the eight (8) pyrazine derivatives obtained from Sigma Aldrich and designated as **A-H** were used for this study. 0.2 wt % of each pyrazines were prepared and used for the experiment. The molecular structures of the pyrazine molecules are shown in Fig. 1.

2.2. Immersion Tests (Weight Loss)

Weight loss tests were carried out on X60 steel specimens in 15 % HCl without and with 0.2 wt % concentration of each pyrazine molecules immersed up to 24 h at 25°C. Weighing of each specimen was carried out before immersion. The coupons were retrieved after 24 h, immersed in 1 M HCl for 15 s to get rid of any corrosion products, washed thoroughly, dried in air, and re-weighed. The corrosion rates were evaluated in mils per year (mpy) and mm per year (mm/y) as shown in the following equations [48].

$$\text{Corrosion rate (mpy)} = \frac{3.45 \times 10^6 \times W}{D \times A \times T} \quad (1)$$

$$\text{Corrosion Rate (mm/y)} = \frac{W \times 8.76 \times 10^4}{A \times T \times D} \quad (2)$$

Where W is weight loss in (g), A is the initial exposed area of the coupon (cm^2), T is the exposure time in hours (h) and D is the density of the metal coupon (7.86 g/cm^3).

Corrosion inhibition efficiency which gives the measure of the effectiveness of the inhibitor was calculated using equation 3 [49]:

$$\text{Inhibitor Efficiency, \%IE} = \frac{Cr_B - Cr_I}{Cr_B} \times 100 \quad (3)$$

Where Cr_B is the corrosion rate (mpy) without inhibitor and Cr_I is the corrosion rate (mpy) with inhibitor present.

2.3. Computational details

Density functional theory (DFT) using B3LYP with 6-31G** basis set method available in Spartan 14 software package was utilized to carry out geometry optimization of the eight pyrazine molecules investigated. The DFT calculations were conducted in the presence of water since corrosion takes place in aqueous phase.

DFT is an authentic and powerful tool for analyzing mechanisms during inhibitor-surface interactions. Based on the frontier molecular orbital theory, the chemical reactivity of a chemical specie is as a result of the interaction between the lowest unoccupied molecular orbital (LUMO) and the highest occupied molecular orbital (HOMO) of the reacting species. The parameter associated with the electron donating ability in the quantum calculations is known as energy of the highest occupied molecular orbital (E_{HOMO}) while the molecular orbital which is associated with the ability of the molecule to accept electrons is known as the energy of the lowest unoccupied molecular orbital (E_{LUMO}).

The corrosion inhibition efficiency was measured experimentally from weight loss test. The energy gap, ΔE ($E_{\text{LUMO}} - E_{\text{HOMO}}$), is a critical descriptor and it shows the reactivity of the inhibitor molecules. The distance between two bonded atoms and the product of the charge on the atoms is known as the dipole moment (DM). The dipole moment gives a measure of the polarity of a polar covalent bond. It is widely used in describing the polarity of molecules. The measure of solubility or the partitioning of an organic compound between a polar and a non-polar phases is termed LogP. Qualitative chemical concepts such as softness (s), global electrophilicity (ω), chemical hardness (η), electronegativity (χ) and local reactivities were also obtained from DFT calculations.

The chemical potential and electronegativity are related as presented in equation 4 [50]:

$$\mu = \frac{dE}{dn} V(r) = -\chi = -\frac{IP+EA}{2} = \frac{E_{HOMO}+E_{LUMO}}{2}, \quad (4)$$

Where E is the total energy, μ is the chemical potential, n is the number of electrons and V(r) is the external potential of the system. The second derivative of energy with respect to n is the chemical potential. This measures the reactivity and stability of the molecule and it is defined in DFT according to equation 5 [51,52].

$$\eta = \frac{d^2E}{d^2n} V(r) = \frac{IP-EA}{2} = \frac{E_{LUMO}-E_{HOMO}}{2} \quad (5)$$

Where EA is electron affinity and IP is ionization potential.

Softness (s) and global electrophilicity index (ω) are calculated as presented in equations 6 and 7, respectively [53–55].

$$s = \frac{1}{2\eta} \quad (6)$$

$$\omega = \frac{\mu^2}{2\eta} \quad (7)$$

The number of electrons transferred between the metal surface and the molecule (ΔN) is evaluated from equation 8 [56].

$$\Delta N = \frac{\chi_{metal}-\chi_{molecule}}{2(\eta_{metal}+\eta_{molecule})} = \frac{\phi-\chi_{molecule}}{2\eta_{molecule}} \quad (8)$$

Where ϕ is work-function (4.82 eV) [50,51] and is taken as the electronegativity of the metal. The chemical hardness of the metal is neglected because the chemical hardness of bulk metals is related to the inverse of their density of states at the Fermi level which is very small and χ is the electronegativity.

2.4. Quantitative Structural Activity Relationship (QSAR)

The structure-activity relationship of molecular descriptors from the quantum chemical calculations of the various pyrazine molecules was developed utilizing multiple linear regression. The quality of the model in this analysis relies on the prediction ability and fitting. Various quantum chemical descriptors such as E_{HOMO} , E_{LUMO} , dipole moment, log P, molecular volume etc., were computed and used for correlation with the corrosion inhibition efficiencies of the eight pyrazines determined experimentally. The relationship to evaluate the correlation between observed activity and molecular descriptors was sought using an equation. Multiple linear regression analysis is frequently used to correlate the quantum molecular descriptors with experimental inhibition efficiency. The obtained data was categorized into various sets to be able to formulate a QSAR model and the workability of the model.

$$\%IE = \alpha + \beta_1 X_1 + \beta_2 X_2 + \beta_3 X_3 + \dots \dots \dots \beta_n X_n \quad (9)$$

Where α and β are regression constants determined through multiple linear regression analysis, $X_1, X_2, X_3, \dots, X_n$ are quantum chemical index characteristics of the various molecules.

It is vital to determine the coefficient of correlation of the molecular descriptors in order to develop a QSAR model with good reliability. Step-wise regression analysis was utilized for searching and developing the best QSAR models to establish the important descriptors that were involved in inhibiting corrosion. Two-tailed t-tests (t -statistics) was used to evaluate the significance of each parameter in a stepwise manner. The overall significance of the model was tested using F-test. Other

statistical parameters such as squared correlation adjusted coefficient (R^2_{adj}), P-value and squared correlation coefficient (R^2), were used to validate the model at 95% confidence interval. The step-wise regression analyses were carried out using XLSTAT, statistical software for Excel 2013.

3. RESULTS AND DISCUSSION

3.1. Weight Loss measurements

Corrosion rates and inhibition efficiencies of the eight (8) investigated pyrazines in 15 % HCl without and with 0.2 wt% concentration after immersion of the steel coupons for 24 h at 25°C are presented in Table 1.

Table 1. Weight loss results for X60 steel in 15 % HCl with and without different pyrazines derivatives at 25 °C after 24 h of immersion at an inhibitor concentration of 0.2 wt%.

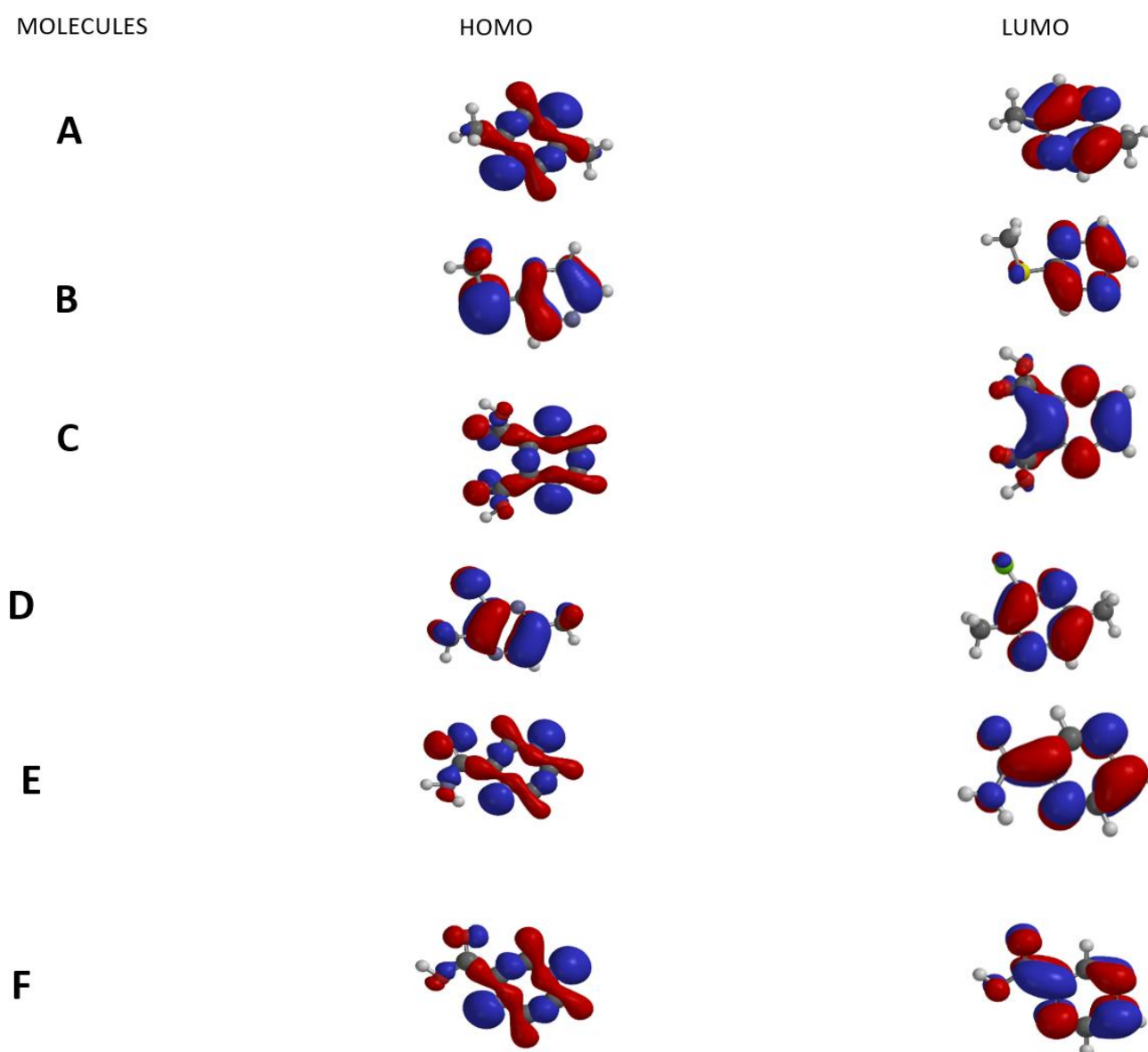
Inhibitor	Weight Loss (g)	Corrosion Rate mpy	Corrosion Rate mm/y	Inhibitor Efficiency, % IE
Blank	0.2377	144.90	3.6794	-
PYR A	0.1839	112.11	2.8466	22.63
PYR B	0.1611	98.21	2.4937	32.22
PYR C	0.1234	75.23	1.9101	48.08
PYR D	0.1376	83.88	2.1299	42.11
PYR E	0.0838	51.12	1.2979	64.72
PYR F	0.1064	64.86	1.6470	55.24
PYR G	0.1340	81.69	2.0742	43.62
PYR H	0.1798	109.61	2.7832	24.35

The results show that all the derivatives of pyrazine studied protected the steel to various extents. Pyrazine E exhibited the highest inhibition efficiency of 64.72% and also has the lowest corrosion rate of 51.12 mpy as compared to the blank (15% HCl) with a value of 144.90 mpy. On the other hand, pyrazine A was the worst inhibitor with an inhibition efficiency of 22.63%. The high inhibition efficiency of Pyrazine E is due to the presence of amide group $-\text{CO}-\text{NH}_2-$ on the pyrazine ring as compare to pyrazine A which only has two methyl groups $-\text{CH}_3$ attached to the pyrazine ring. This amide group induces high polarity and increase the molecular volume of pyrazine E which can adsorbed more strongly to the steel surface than pyrazine A.

3.2. Molecular Descriptors

Molecular parameters of the molecules under investigation give a useful insight into the reactivity and selectivity of the molecules. These parameters provide useful information that can be utilized in comparing reactivity trends among different molecules. It is also important in understanding metal

surface - inhibitor the interactions [57]. The useful molecular descriptors identified in this study are as follows; E_{HOMO} , the energy of the highest occupied molecular orbital, E_{LUMO} , the energy of the lowest unoccupied molecular orbital, ΔE , the energy difference between E_{LUMO} and E_{HOMO} , the dipole moment (DM), chemical potential (μ), chemical hardness (η), softness (s), global nucleophilicity (ω) and electronegativity (χ) etc,. Information regarding the areas of the molecule with the most energetic electrons is given by the highest occupied molecular orbital (HOMO) while information regarding areas in the molecule that exhibits the highest tendency to accept electrons are given by the lowest unoccupied molecular orbital (LUMO). The HOMO and LUMO orbitals overlay are illustrated in Figure 2. The results from Fig. 2 indicate that the HOMO and LUMO regions for all the eight pyrazines investigated are located on the pyrazine ring. This indicates that the pyrazine ring is the active site for the interaction between the molecules and the steel surface,



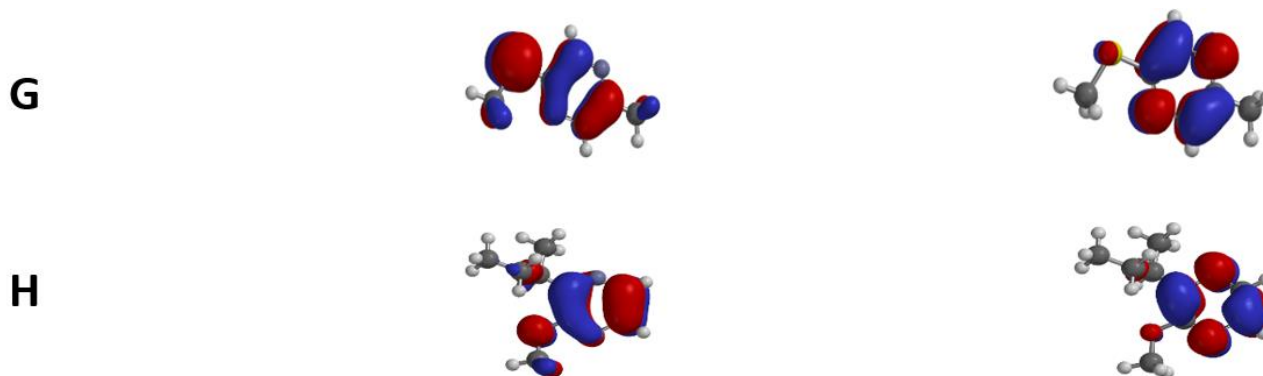


Figure 2. The highest occupied molecular orbital and the lowest unoccupied molecular orbital for the eight pyrazine molecules A-H investigated.

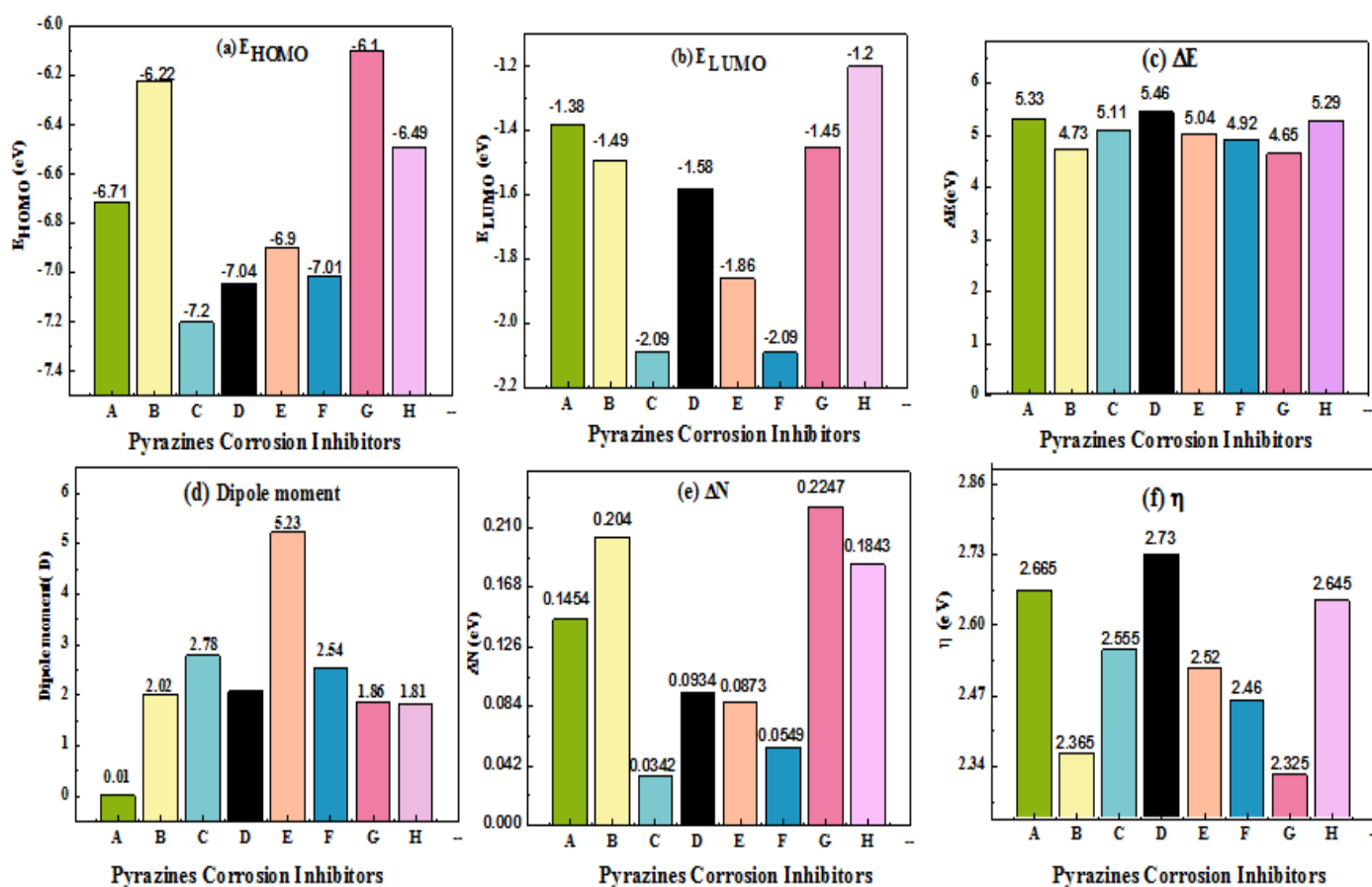


Figure 3. Quantum chemical parameters and descriptors (a) E_{HOMO} , (b) E_{LUMO} (c) ΔE , (d) dipole moment (e) ΔN and (f) hardness obtained using DFT at B3LYP/6-31G** level of theory for the eight pyrazine molecules A-H investigated.

The ability of the molecule to bind with the surface of the metal is expected to increase with increasing HOMO and decreasing LUMO energy values [58–60]. The higher the value of E_{HOMO} , the more a molecule can donate its electrons. The E_{HOMO} values evaluated at the B3LYP/6-3G level of theory

for the investigated pyrazines is illustrated in Table 2 and Fig. 3a, respectively. Corrosion efficiencies of the molecules obtained from weight loss experiment are presented in Table 2, the trend in the E_{HOMO} values of the molecules does not agree with experimentally determined corrosion inhibition efficiencies of the pyrazine corrosion inhibitors investigated.

E_{LUMO} gives information about the electron accepting ability of a molecule. The lower E_{LUMO} , the greater the ability of the molecule to accept electrons. E_{LUMO} values obtained are presented in Table 2 and Fig. 3(b). It can be observed that trends in E_{LUMO} values of the molecules are not in agreement with the observed inhibition efficiency [54,55].

Table 2. Quantum Chemical Descriptors for Pyrazine Derivatives Investigated

Parameters	A	B	C	D	E	F	G	H
Energy (au)	-342.97	-701.83	-641.44	-802.57	-433.05	-452.90	-741.16	-536.13
E_{HOMO} (eV)	-6.71	-6.22	-7.20	-7.04	-6.90	-7.01	-6.10	-6.49
E_{LUMO} (eV)	-1.38	-1.49	-2.09	-1.58	-1.86	-2.09	-1.45	-1.20
ΔE (eV)	5.33	4.73	5.11	5.46	5.04	4.92	4.65	5.29
η	2.66	2.36	2.55	2.73	2.52	2.46	2.32	2.64
s	0.18	0.21	0.19	0.18	0.19	0.20	0.22	0.19
μ	-4.05	-3.86	-4.65	-4.31	-4.38	-4.55	-3.78	-3.85
χ	4.05	3.86	4.65	4.31	4.38	4.55	3.78	3.85
ω	3.07	3.14	4.22	3.40	3.81	4.21	3.06	2.79
ΔN	0.15	0.20	0.03	0.09	0.08	0.05	0.22	0.18
Dipole Moment (D)	0.01	2.02	2.78	2.07	5.23	2.54	1.86	1.81
LogP	-0.24	0.52	-0.68	0.66	-1.31	-0.66	0.72	1.79
Polarizability	50.10	50.33	51.74	51.18	49.72	49.51	51.84	55.31
Molecular Volume (\AA^3)	123.16	124.22	142.73	136.79	117.55	114.59	142.56	187.22
Molecular Area (\AA^2)	144.98	146.01	167.47	159.86	139.52	136.23	166.43	212.68
%IE	22.63	32.22	48.08	42.11	64.72	55.24	43.62	24.35

The energy difference between the HOMO and the LUMO (ΔE) gives information about the overall reactivity of a molecule; the smaller the ΔE value, the greater the reactivity of the molecule. The trends in the ΔE values for the molecules studied as presented in Table 2 and Fig. 3c, indicate that pyrazine D (5.46 eV) should have been the least reactive compound while pyrazine G (4.65 eV) the most reactive molecule [61–64]. As a result, the highest interaction between the metal surface and the molecule expected should have been pyrazine G. The overall trend in the E_{LUMO} , ΔE , and E_{HOMO} values of these molecules indicate no correlation with the trend in the corrosion inhibition efficiency.

The dipole moment indicates the degree of polarity of the molecule which is a good indicator of reactivity [41,65,66]. Clearly, there is no correlation between the observed efficiency and the dipole

moment of the molecules studied as illustrated in Table 2 and Fig. 3d. The ability of the molecule to donate electrons is given by the number of electrons transferred (ΔN). The higher the value of ΔN is, the greater the tendency of a molecule to donate electrons. In the case of corrosion inhibitors, a higher ΔN implies a greater interaction between the molecule and the metal leading to an increase in the efficiency [67–69]. This is, however, not the case in this work; the trend in the ΔN values has no correlation with the experimentally obtained corrosion inhibition efficiency for the pyrazine derivatives investigated. Similarly, there is no correlation in the hardness (Table 2 and Fig. 3e), molecular volume, molecular area, logP, and the experimental values of the corrosion inhibition efficiencies for the eight (8) pyrazine derivatives as shown in Table 2.

3.3. QSAR Modeling

In it apparent from the quantum chemical calculation data from the previous section that there is lack of correlation between each molecular descriptor with the experimentally determined inhibition efficiencies of the pyrazines. In order to obtain a trustworthy model of efficiency - structure relationship on corrosion inhibition, a composite index of more than one parameter should be used to set up a quantitative structure-activity relationship known as QSAR. The significance of the developed QSAR model will depends largely on the fitting and its ability to predict the corrosion inhibitor efficiency [1,51,70,71].

A step-wise process was adopted in developing the QSAR for this study. In the stepwise process, the correlation coefficients of all the descriptors were determined individually using the linear regression as presented in Table 3. The descriptor with the largest absolute t-value was selected and the descriptor associated with the model is selected as the best single predictor of inhibition efficiency in the first step. Dipole moment (DM) was the only descriptor that was significant in predicting the corrosion inhibition efficiency independently. To be able to get an appropriate model that is significant in predicting the inhibition performance, an attempt was made to form a QSAR model by combining the various molecular parameters. The regression equation obtained at this stage is given as

$$\% IE = 21.71 + 8.69 DM \quad (10)$$

In the second step, all possible two-predictor regression models with DM as one of the independent variables in the model was examined. Here the other descriptors in conjunction with DM that produces the largest absolute value of t in the model are determined. The equation of the model at this stage is given as;

$$\% IE = -6.30 + 5.97 DM - 20.86 E_{LUMO} \quad (11)$$

At this stage, the t values of DM and E_{LUMO} are examined and the significance of the model is as illustrated in Table 4.

Having gone through several selections and t-tests to ascertain the significance, a QSAR model was obtained involving Dipole moment (DM), E_{LUMO} (eV), and Molecular Volume (\AA^3) that predicts the corrosion inhibition efficiency as presented in Table 5. The process ends when the t-value obtained becomes insignificant after adding new descriptors. The obtained regression model is illustrated in equation 12.

$$\%IE = 14.288 + 6.185DM - 16.464ELUMO - 0.102MV \quad (12)$$

Where E_{LUMO} (eV) is the energy of the lowest unoccupied molecular orbital, DM is the dipole moment (Debye) and MV (\AA^3) is the molecular volume. The model was utilized to predict inhibitor efficiency of new designed pyrazine derivatives. The predicted efficiency was compared to the efficiency obtained experimentally as presented in Table 6 and Fig. 4.

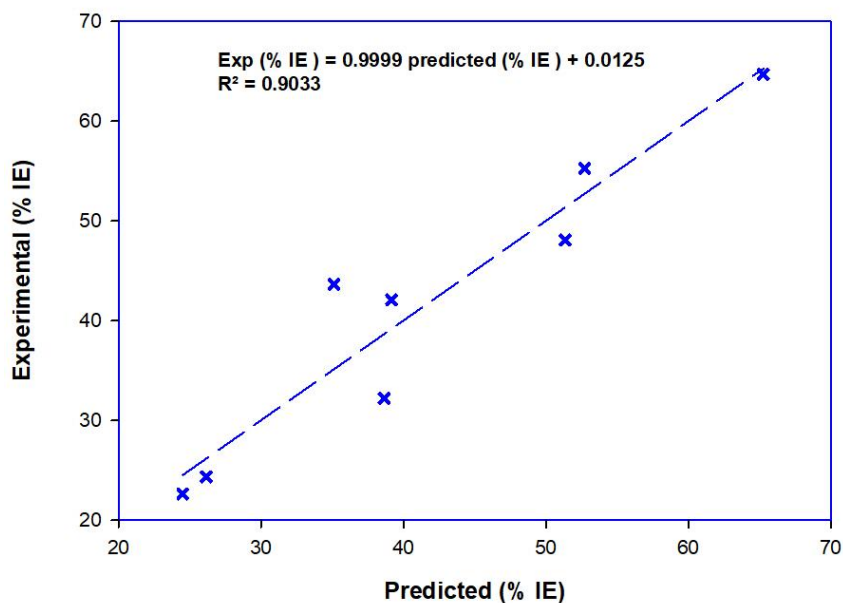


Figure 4. The experimental inhibition efficiency versus predicted data according to equation (12)

3.4. Test Set

Based on the data and information from the training set, a set of new molecules were designed, and the molecular descriptors calculated [72]. The QSAR model obtained from the training set was then utilized in predicting corrosion inhibition efficiency of the new set of molecules. The QSAR model obtained from the training set indicates that the inhibition efficiency of pyrazines is dependent on Dipole moment (DM), E_{LUMO} (eV), and Molecular Volume (\AA^3). The molecular structures of the new molecules designed are illustrated in Figure 5. The molecular descriptors calculated using the B3LYP/6-31G** level of theory are presented in Table 7. As illustrated in Table 7, it was observed that the corrosion inhibition efficiency increases with increasing dipole moment. This phenomena has been observed by various authors [17,73–75], even though there has not been any consensus as to the effect of dipole moment on the inhibition efficiency entirely [76–78].

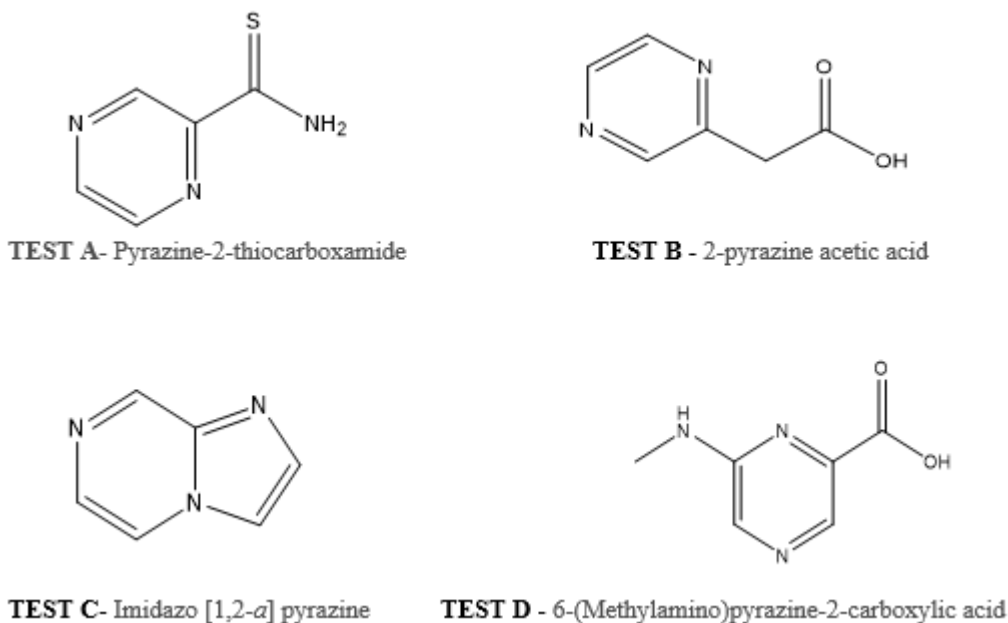


Figure 5. 2 D-molecular structures of the designed molecules.

Dipole moment can be valuable in predicting the adsorption mechanism [79]. The electrostatic interaction between the charged centers of the molecule and that of the metal surface results in a positive dipole interaction of the metal surface and the molecule. In this light, the positive coefficient of dipole moment obtained suggests that the adsorption is through physical mechanism [77,78,80].

4. CONCLUSION

In conclusion, the corrosion inhibition performances of eight different pyrazine molecules were investigated using a combined weight loss experiment and DFT calculations. Step-wise regression analysis was used to correlate the molecular parameters obtained from DFT calculations to the corrosion inhibition efficiency obtained from weight loss test. QSAR model was developed that correlates the dipole moment, molecular volume and E_{LUMO} to the inhibition efficiency obtained from weight loss with 90% correlation. The QSAR model was utilized to predict the corrosion inhibition efficiency of test molecules designed with pyrazine backbone.

ACKNOWLEDGMENTS

The authors would like to acknowledge the support received from King Abdulaziz City for Science and Technology (KACST) for funding this work under the National Science Technology Plan (NSTIP) grant No. 14-ADV2448-04. Also, the support provided by the Deanship of Scientific Research (DSR) and the Center of Research Excellence in Corrosion (CORE-C), at King Fahd University of Petroleum & Minerals (KFUPM) is gratefully acknowledged.

References

1. S.G. Zhang, W. Lei, M.Z. Xia and F.Y. Wang, *J. Mol. Struct.: Theochem* 732 (2005) 173.
2. A. Popova, M. Christov and A. Zvetanova, *Corros. Sci.* 49 (2007) 2131.
3. A.A. Farag and T.A. Ali, *J. Ind. Eng. Chem.* 21 (2015) 627.
4. A.O. James, N.C. Oforika, O.K. Abiola and B.I. Ita, 32 (2007) 31.
5. A.A. Al-taq, S. Aramco, S.A. Ali and K. Fahd, *SPE J.* (2009) 627.
6. G. Avci, *Colloids Surfaces A Physicochem. Eng. Asp.* 317 (2008) 730.
7. F. Bentiss, M. Traisnel, L. Gengembre, M. Lagrenée, *Appl. Surf. Sci.* 161 (2000) 194.
8. K.R. Ansari, D. S. Chauhan, M. A. Quraishi and T.A. Saleh, *J. Coll. Inter. Sci.* 564 (2020) 124.
9. K.M. Ismail, *Electrochim. Acta.* 52 (2007) 7811.
10. A.K. Singh and M.A. Quraishi, *Corros. Sci.* 52 (2010) 152.
11. C. Hao, R.H. Yin, Z.Y. Wan, Q.J. Xu and G.D. Zhou, *Corros. Sci.* 50 (2008) 3527.
12. L. Wang, *Corros. Sci.* 43 (2001) 2281.
13. A. Popova, M. Christov, S. Raicheva and E. Sokolova, *Corros. Sci.* 46 (2004) 1333.
14. G. Moretti, *Electrochim. Acta.* 41 (1996) 1971.
15. M. Dündükcü, B. Yazici and M. Erbil, *Mater. Chem. Phys.* 87 (2004) 138.
16. M. Kissi, M. Bouklah, B. Hammouti and M. Benkaddour, *Appl. Surf. Sci.* 252 (2006) 4190.
17. S.K. Saha, A. Hens, A. Roychowdhury and A.K. Lohar, *Can. Chem. Trans.* 2 (2014) 489.
18. S.C. Rasmussen, R.L. Schwiderski and M.E. Mulholland, *Chem. Commun.* 47 (2011) 11394.
19. J. Li, Q. Li and D. Liu, *ACS Appl. Mater. Interfaces.* 3 (2011) 2099.
20. T. Akiyama, Y. Enomoto and T. Shibamoto, *J. Agric. Food Chem.* 26 (1978) 1176.
21. T.B. Adams, S.M. Cohen, J. Doull, V.J. Feron, J.I. Goodman, L.J. Marnett, I.C. Munro, P.S. Portoghese, R.L. Smith, W.J. Waddell and B.M. Wagner, *Food Chem. Toxicol.* 43 (2005) 1207.
22. T. Guilford, C. Nicol, M. Rothschild and B.P. Moore, *Biol. J. Linn. Soc.* 31 (1987) 113.
23. R. Goel, V. Luxami, K. Paul, *Org. Biomol. Chem.* 4 (2010) 1166.
24. W.W.K.R. Mederski, D. Kux, M. Knoth and M. J. Schwarzkoph-Hofmann, *Heterocycles*, 60 (2003) 925.
25. P.J. Steel and C.M. Fitchett, *Coord. Chem. Rev.* 252 (2008) 990.
26. Y. Higashio and T. Shoji, *Appl. Catal. A Gen.* 260 (2004) 251.
27. M. Bouklah, A. Attayibat, S. Kertit, A. Ramdani and B. Hammouti, *Appl. Surf. Sci.* 242 (2005) 399.
28. D.L. Du, D.A. Volpe, C.K. Grieshaber and M.J. Murphy Jr., *Invest. New Drugs.* 9 (1991) 149.
29. A. Rey, C. Gouedard, N. Ledirac, M. Cohen, J. Dugay, J. Vial, V. Pichon, L. Bertomeu, D. Picq, D. Bontemps, F. Chopin and P.L. Carrette, *Int. J. Green house Gas Control.* 19 (2013) 576.
30. E.J. Moran, O.D. Easterday and B.L. Boser, *Drug Chem. Toxicol.* 3 (2015) 249.
31. J.J. Kaminski, D.G. Perkins, J.D. Frantz, D.M. Solomon, A.J. Elliott, P.J.S. Chiu and J.F. Long, *J. Med. Chem.* 30 (1987) 2047.
32. R.T. Vashi, H.M. Bhajiwala and S.A. Desai, *Der Pharma Chem.* 5 (2013) 237.
33. S. Deng, X. Li and H. Fu, *Corros. Sci.* 53 (2011) 822.
34. I.B. Obot and Z.M. Gasem, *Corros. Sci.* 83 (2014) 359.
35. H. Zhu, X. Chen, X. Li, J. Wang, Z. Hu and X. Ma, *J. Mol. Liq.* 297 (2020) 111720.
36. R. Farahati, S. M. Mousavi-Khoshdeld, A. Ghaffarinjad and H. Behzadi, *Prog. Org. Coat.* 142 (2020) 105567 .
37. I. Danaee, O. Ghasemi, G.R. Rashed, M.R. Avei and M.H. Maddahy, *J. Mol. Struct.* 1035 (2013) 247.
38. M.A. Migahed, E.A. Khamis and E.G. Zaki, *J. Mol. Liq.* 212 (2015) 360.
39. A. Kokalj, *Corros. Sci.* 53 (2011) 909.
40. L.C. Murulana, M.M. Kabanda and E.E. Ebenso, *J. Mol. Liq.* 215 (2016) 763.
41. A. Jmiai, B. El Ibrahim, A. Tara, S. El Issami, O. Jbara and L. Bazzi, *J. Mol. Struct.* 1157 (2018) 408.

42. F. Bentiss, M. Lebrini, H. Vezin, F. Chai, M. Traisnel and M. Lagrené, *Corros. Sci.* 51 (2009) 2165.
43. M. Lebrini, M. Traisnel and M. Lagrene, *Corros. Sci.* 50 (2008) 473.
44. H. Vezin and M. Traisnel, *Corros. Sci.* 49 (2007) 2254.
45. M. Lebrini and F. Bentiss, *Corros. Sci.* 48 (2006) 1279.
46. H. Vezin and L. Gengembre, *Corros. Sci.* 47 (2005) 485.
47. F. Bentiss, M. Traisnel, H. Vezin and M. Lagrene, *Corros. Sci.* 45 (2003) 371–380.
48. I.B. Obot, N.K. Ankah, A. Sorour, Z.M. Gasem and K. Haruna, *Sustain. Mater. Technol.* 14 (2017) 1.
49. K. Haruna, I.B. Obot, N.K. Ankah, A.A. Sorour and T.A. Saleh, *J. Mol. Liq.* 264 (2018) 515–525.
50. L. Li, X. Zhang, S. Gong, H. Zhao and Y. Bai, *Corros. Sci.* 99 (2015) 76.
51. R.L. Camacho-mendoza, E. Gutie, J.A. Rodr and J.G. Alvarado-Rodr, *J. Chem. Inf. Model.* 55 (2015) 2391.
52. A.S. Fouda, M.A. Ismail and A.S. Abousalem, *J. Mol. Liq.* 240 (2017) 372.
53. A.K. Oyebamiji and B. Semire, *Int. J. Corros. Scale Inhib.* 5 (2016) 248.
54. H. Behzadi, P. Roonasi, M. Jafar, S. Manzetti, M.D. Esrafil, I.B. Obot, M. Yousefvand and S.M. Mousavi-khoshdel, *J. Mol. Struct.* 1086 (2015) 64.
55. M.E. Mashuga, L.O. Olasunkanmi and E.E. Ebenso, *J. Mol. Struct.* 1136 (2017) 127.
56. I.B. Obot, D.D. Macdonald and Z.M. Gasem, *Corros. Sci.* 99 (2015) 1.
57. B. El Ibrahim, A. Soumoue, A. Jmiai, H. Bourzi, R. Oukhrib, K. El Mouaden, S. El Issami and L. Bazzi, *J. Mol. Struct.* 1125 (2016) 93.
58. K. Sayin, N. Kurtoglu, M. Kose and D. Karakas, *J. Mol. Struct.* 1119 (2016) 413.
59. T. Pandiyan, *J. Mol. Struct.* 1119 (2016) 314.
60. E. Saban, S.S. Zaki, K. Savas, O.I. Dilara, L. Guo and K. Cemal, *J. Mol. Struct.* 1134 (2017) 751.
61. F.E. Heakal, S.K. Attia, S.A. Rizk, M.A.A. Essa and A.E. Elkholy, *J. Mol. Struct.* 1147 (2017) 714.
62. E.E. Elemike, H.U. Nwankwo, D.C. Onwudiwe and E.C. Hosten, *J. Mol. Struct.* 1141 (2017) 12.
63. H.R. Obayes, A.A. Al-amiery, G.H. Alwan, T. Adnan, A. Amir, H. Kadhum and A. Bakar, *J. Mol. Struct.* 1138 (2017) 27.
64. S. Rani, P. Mourya, M.M. Singh and V.P. Singh, *J. Mol. Struct.* 1137 (2017) 240.
65. H. Behzadi and A. Forghani, *J. Mol. Struct.* 1131 (2017) 163–170.
66. H. Behzadi, S. Manzetti, M. Dargahi and P. Roonasi, *J. Mol. Struct.* 1151 (2018) 34.
67. K. Benbougerra, S. Chafaa, N. Chafai and M. Mehri, *J. Mol. Struct.* 1157 (2018) 165.
68. E.E. Elemike, H.U. Nwankwo and D.C. Onwudiwe, *J. Mol. Struct.* 1155 (2018) 123.
69. F.E. Heakal, S.A. Rizk and A.E. Elkholy, *J. Mol. Struct.* 1152 (2018) 328.
70. X. Kong, C. Qian, W. Fan and Z. Liang, *J. Mol. Struct.* 1156 (2018) 164.
71. L. Dinparast, H. Valizadeh, M. Babak and S. Soltani, *J. Mol. Struct.* 1114 (2016) 84.
72. M.A. El-raouf, E.A. Khamis, M.T.H. Abou and N.A. Negm, *J. Mol. Liq.* 255 (2018) 341.
73. F. Ahmad, M. Jane, M. Alam, S. Azaz, M. Parveen, S. Park and S. Ahmad, *J. Mol. Struct.* 1151 (2018) 327.
74. P. Xuehui, G. Min, Z. Yuxuan, W.E.I. Qin and H.O.U. Baorong, *Sci. China.* 54 (2011) 1529.
75. R. G. Sundaram and M. Sundaravadivelu, *Egypt. J. Pet.* (2017) 1.
76. I.B. Obot, A. Madhankumar, S.A. Umoren and Z.M. Gasem, *J. Adhes. Sci. Technol.* 29 (2015) 2130.
77. V.S. Sastri, *Green Corrosion Inhibitors*, John Wiley & Sons, Ltd, 2011.
78. C. Verma and M.A. Quraishi, *J. Assoc. Arab Univ. Basic Appl. Sci.* 23 (2017) 29.
79. E. Ituen, O. Akaranta and A. James, *J. Mol. Liq.* 224 (2016) 408.

80. K. Bahgat and A.G. Ragheb, *Cent. Eur. J. Chem.* 5 (2007) 201.

© 2020 The Authors. Published by ESG (www.electrochemsci.org). This article is an open access article distributed under the terms and conditions of the Creative Commons Attribution license (<http://creativecommons.org/licenses/by/4.0/>).